Supplementary Information for

Mechanistic Insights of Ru nanoparticles *in situ* formation during hydrodeoxygenation of lignin-derived substances to hydrocarbons

Evgeny R. Naranov,[a] Alexey A. Sadovnikov [a], Olga V. Arapova,[a] Aram L. Bugaev,[b] Oleg A. Usoltsev,[b] Dmitry N. Gorbunov,[a] Vincenzo Russo,[c] Dmitry Yu. Murzin,[d] Anton L. Maximov [a]*

[a] Topchiev Institute of Petrochemical Synthesis, Russian Academy of Sciences, Leninsky prospekt, bld. 29, 119991, Moscow, Russia

E-mail: naranov@ips.ac.ru

[b] The Smart Materials Research Institute, Southern Federal University, Sladkova Street 178/24, Rostov-on-Don 344090, Russia

[c] Universita degli Studi di Napoli "Federico II", 80138, Naples, Italy

[d] Åbo Akademi University, Henriksgatan 2, Turku/Åbo, 20500, Finland

Corresponding author: Evgeny R. Naranov: naranov@ips.ac.ru,

Phone: +7 (495) 955 4125 (3-49)

EXPERIMENTAL SECTION

Catalytic experiments

Hydrogenation of oxygen-containing substances (guaiacol or diphenyl ether - DPhE) was conducted in a steel autoclave equipped with a magnetic stirrer and a pressure gauge. The autoclave was charged with 0.050 g of catalyst and 2 ml of the substrate solution. In a typical experiment, a catalyst with guaiacol (10 wt. % in n-$C_{12}H_{34}$) or DPhE solution (10 wt. % in n-$C_{16}H_{34}$) was put in the autoclave with the inner

volume of 10 ml. The autoclave was filled with hydrogen to a pressure of 50 bar. The reaction was run at 423-573 K with a stirrer speed of 700 rpm. After the reaction, the autoclave was cooled to room temperature and the pressure was decreased to the atmospheric. The error bars are based on at least triplicate experiments.

The qualitative composition of the liquid products was determined by gas chromatography - mass spectrometry using a Finnigan MAT 95 XL instrument equipped with a Varian VF-5MS capillary column and helium as a carrier gas (1.5 cm3/min). Temperature programming was conducted as follows: holding at 307 K for 5 min, heating to 563 K (10 K/min), holding for 10 min. The concentrations of the products were calculated by the ratio between the corresponding peak areas and total chromatogram areas considering the response factors of pure substances. The results were processed using the Xcalibur software package. The products were identified by matching their mass spectra against the dedicated mass spectra library of the software

Characterization

The textural characteristics of the samples were determined by low-temperature nitrogen adsorption (77 K) using a Micromeritics ASAP 2020 instrument. Prior to analysis, the samples were evacuated at 623 K for 6 h. The specific surface area was calculated by BET; the pore size distribution was calculated according to the Barrett–Joyner–Halenda (BJH) model using adsorption data following the approach proposed by Ryoo and co-workers.[1] For RuO_2/ZSM-5 and RuO_2/ZM the NLDFT and Horvath-Kawazoe method was applied.

The composition of the samples was analyzed by atomic absorption spectrometry using a PerkinElmer Analyst instrument.

X-ray powder diffraction analysis was carried out using a Rigaku D/MAX 2500 diffractometer (CuKα radiation) in the 2θ range of 1–50°, with a goniometer rotation speed of 1° min−1.

Temperature-programmed reduction with hydrogen (TPR-H2) was performed with an AutoChem 2950HP instrument (Micromeritics Instrument Corp., Norcross, GA, USA). Before the analysis, the catalyst was oxidized at 673 K for 60 min under air flow followed by scavenging with Ar flow at 673 K for 1 h and cooling down to 323 K. The reduction was performed under 20 mL/min flow of 10 vol. % H2–90 vol. % Ar mixture in the temperature range of 323 – 673 K with a ramp of 10 K/min.

Acidity of porous samples was determined using a USGA-101 instrument. A sample was exposed to a nitrogen stream at 673 K for 1 h. Saturation was conducted in a stream of nitrogen diluted dry ammonia at a temperature of 333 K for 15 min. Physically adsorbed ammonia was removed in a dry helium stream at 373 K at a nitrogen purge flow rate of 30 cm^3/min for 1 h. To record a temperature-programmed desorption (TPD) curve, the sample was cooled to 323 K, and then the temperature was gradually increased up to 773 K at a rate of 8 K/min. Signals from the thermal conductivity detector and the temperature sensor were concurrently recorded through a multichannel ADC using the ECOCHROM software program.

TGA was performed on Mettler TA 4000 system. The heating and cooling of samples was performed at a rate of 10 K/min under air flow of (70 mL/min) in the range of 20 °C to 800 °C.

For transmission electron microscopy (TEM) FEI's Tecnai Osiris TEM with an accelerating voltage of 200 keV was used.

Scanning electron microscopy (SEM) images and energy-dispersive X-ray (EDX) spectra were recorded using an NVision 40 microscope (Carl Zeiss) equipped with the X-Max 80 EDX detector (Oxford Instruments).

Enthalpy and Gibbs free energy changes calculations

Enthalpy (ΔH^0_r) and Gibbs free energy (ΔG^0_r) at standard conditions were calculated by following a thermodynamic approach [1], starting from the standard enthalpy (ΔH^0_f) and Gibbs free energy (ΔG^0_f) of formation from the elements estimated with Joback approach [2-4], Eq. 1-2.

$$\Delta H^0_{r,j} = \sum_j \nu_{i,j} \cdot \Delta H^0_{f,i} \quad (1)$$

$$\Delta G^0_{r,j} = \sum_j \nu_{i,j} \cdot \Delta G^0_{f,i} \quad (2)$$

The equilibrium constant of each reaction was calculated from its definition, Eq. 3.

$$K^0_j = \exp\left(-\frac{\Delta G^0_{r,i}}{RT}\right) \quad (3)$$

The dependency of the reaction free Gibbs energy with temperature was included by implementing the Gibbs-Helmholtz equation valid at P=1bar ($\Delta G^{\Phi}_{r,j}$) (Eq. 4).

$$\frac{\Delta G^{\phi}_{r,j}(T)}{T} = \frac{\Delta G^0_{r,j}}{T^0} + \Delta H^0_{r,j}\left(\frac{1}{T} - \frac{1}{T^0}\right) \quad (4)$$

The calculated enthalpy and Gibbs free energy formation for each component (*i*) are reported in Table S1. The stochiometric matrix was built based on the reaction scheme reported in Scheme 1.

Table S1 – Enthalpy and Gibbs free energy formation for each component (*i*) and stochiometric matrix for component *i* for reaction *j*.

Component	*ΔH^0_f [kJ/mol]*	*ΔG^0_f [kJ/mol]*	*i/j*	*1*	*2a*	*2b*	*3a*	*3b*	*4a*	*4b*	*5*	*6*	*7*	*8a*	*8b*	*9a*	*9b*	*10a*	*10b*	*11*
Guaiacol	-260.81	-139.15	**1**	-1	0	0	0	0	0	0	-1	0	-1	0	0	0	0	0	0	0
Methanol	-207.30	-179.28	**2**	1	0	0	0	0	0	0	0	0	0	1	1	0	0	0	0	0
Phenol	-95.32	-32.94	**3**	1	-1	-1	0	0	0	0	0	1	0	0	0	2	0	0	0	0
Cyclohexanol	-292.10	-112.73	**4**	0	1	0	-1	0	-2	0	0	0	0	1	0	0	0	1	0	0
Cyclohexanone	-228.40	-90.79	**5**	0	0	1	0	-1	0	-2	0	0	0	0	1	0	0	-1	-1	0

Cyclohexane	-123.67	31.80	**6**	0	0	0	1	1	0	0	0	0	0	0	0	0	0	1	0
1,1'-bicyclohexyl	-215.30	99.06	**7**	0	0	0	0	0	1	1	0	0	0	0	0	0	0	0	0
1,2-benzenediol	-268.65	-187.56	**8**	0	0	0	0	0	0	0	1	-1	0	0	0	0	0	0	0
Methane	-74.13	-50.79	**9**	0	0	0	0	0	0	0	1	0	0	0	0	0	0	0	0
2-methoxycyclohexanol	-438.28	-217.02	**10**	0	0	0	0	0	0	0	0	0	1	-1	-1	0	0	0	0
Diphenyl ether	49.83	169.98	**11**	0	0	0	0	0	0	0	0	0	0	0	0	-1	-1	0	0	-1
Benzene	81.42	121.68	**12**	0	0	0	0	0	0	0	0	0	0	0	0	0	2	0	0	0
Benzene, (cyclohexyloxy)	-132.38	82.02	**13**	0	0	0	0	0	0	0	0	0	0	0	0	0	0	0	0	1
Water	-241.83	-228.44	**14**	0	0	0	1	1	2	2	0	1	0	0	0	0	2	0	1	0

Starting from these values, the enthalpy, and Gibbs free energy for each reaction (*j*) at standard conditions, equilibrium constants at standard conditions *(K^0_j),* the equilibrium constants (K_j) at different temperatures and pressure were calculated. A temperature range was investigated (T_{min}=423.15K, T_{max}=573.15K). The results of the calculations are reported in Table S2 and Figure 5.

Table S2 – Enthalpy and Gibbs free energy for each reaction (*j*) at standard conditions, equilibrium constants at standard conditions *(K^0_j)*.

Reaction	***ΔH^0_{rxn} [kJ/mol]***	***ΔG^0_{rxn} [kJ/mol]***	***K^0***
1	-41.81	-73.07	6.33E+12
2a	-196.78	-79.79	9.52E+13
2b	-133.08	-57.85	1.36E+10
3a	-73.40	-83.91	5.01E+14
3b	-137.10	-105.85	3.49E+18
4a	-114.76	-132.35	1.54E+23
4b	-242.16	-176.23	7.49E+30
5	-81.97	-99.20	2.39E+17
6	-68.50	-73.82	8.55E+12
7	-177.47	-77.87	4.39E+13
8a	-61.12	-74.99	1.37E+13
8b	2.58	-53.05	1.97E+09
9a	-240.47	-235.86	2.09E+41
9b	-370.66	-383.49	1.53E+67
10a	-63.70	-21.94	6.98E+03
10b	-137.10	-105.85	3.49E+18
11	-182.21	-87.96	2.57E+15

Catalytic experiments

Table S3 - Selectivity over different catalysts. Reaction conditions: *T* 423 K, *P*(H_2) 50 bar.

0.25 hours	RuO_2/ZM	RuO_2/ZSM-5	RuO_2/SBA-15
Conversion, %	48	53	45
2-methoxycyclohexanol	92	90	100
cyclohexanol	8	8	0
cyclohexane	0	2	0
phenol	0	0	0
0.5 hours			
Conversion, %	60	67	70
2-methoxycyclohexanol	88	85	98
cyclohexanol	10	10	0
cyclohexane	2	5	0
phenol	0	0	2
1 hour			
Conversion, %	70	75	80
2-methoxycyclohexanol	87	84	95
cyclohexanol	10	9	0
cyclohexane	3	7	0
phenol	0	0	5

Figure S1 shows the spectra of the RuO_2/ZM catalyst surface over the entire temperature range of the reaction. Intense bands from C-O bonds decrease in intensity with increasing temperature. The band from the carbonyl group persists up to 473 K and (with an increase in temperature) disappears from the spectra and the maximum at 1660 cm^{-1} from double bonds is already intensely manifested. Intense bands from bending vibrations of C-H bonds in the CH_2 and CH_3 groups in the composition of the $C_{12}H_{26}$ solvent and process intermediates are recorded in the spectrum in the region of 1400-1450 cm^{-1}.

The band at 770 cm^{-1}, which is characteristic of a 1,2-substituted aromatic ring with substituents of the same nature, can be attributed to the first intermediate of the hydrogenation process, pyrocatechol, which is characterized by an association of –OH bonds at 3455 cm^{-1} (Fig. 9). The 770 cm^{-1}

band is retained over the entire temperature range of the experiment. The next step is the formation of phenol - bands at 690 and 740 cm^{-1} (ν_{CCH}) in the monosubstituted aromatic ring, which appear in the spectrum up to 473 K.

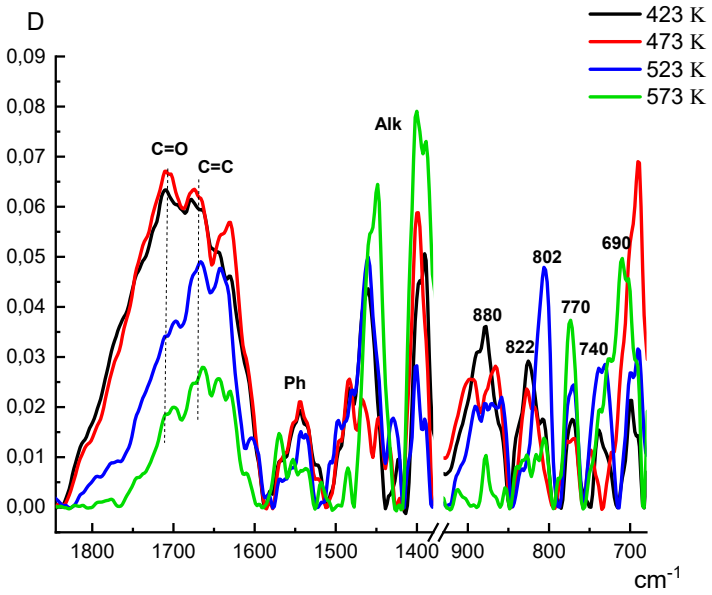

Figure S1. IR spectra of the surface of the RuO_2/ZM catalyst with guaiacol+C12 in the range of 1850-600 cm^{-1}.

The formation of cyclohexane is recorded in the 880 cm^{-1} band; the band refers to the vibrations of the non-planar deformation of the $–CH_2–$ group in the six-membered cycle. The band splits during the experiment, which may indicate the formation of intermediates of cyclohexanol, cyclohexanone, the structure of which is based on the $–CH_2-$ groups in the six-membered paraffin ring.

At 423 K, at the initial moment of the reaction, a less stable conformation of cyclohexane is formed - a "twist-boat" - 822 cm^{-1}, which with an increase in temperature turns into a more stable conformation "chair" - 802 cm^{-1} and further in the entire reaction temperature range up to 573 K with the "chair" conformation is retained.

Figure S2 shows the surface spectra of the RuO_2/ZM catalyst in a flow of DPhE over the entire temperature range of the reaction. At 423 K, benzene shows a sharp intense band at 650 cm^{-1}, which

does not disappear throughout the entire process. Cyclohexenol is associated with a band at 840 cm^{-1}, the intensity of which decreases with temperature, and its isomeric cyclohexanone gives a broad absorption in the region of 1700 cm^{-1}, the intensity of which also gradually decreases with increasing temperature. In the region of 1450 cm^{-1}, the bands are recorded from vibrations of C-H bonds in alkyl groups in the composition of the C16 solvent and intermediates of the hydrogenation process. A wide band of 690 and 730-760 $cm^{-1}$is attributed to all monosubstituted aromatic intermediates of the hydrogenation process and DPhE.

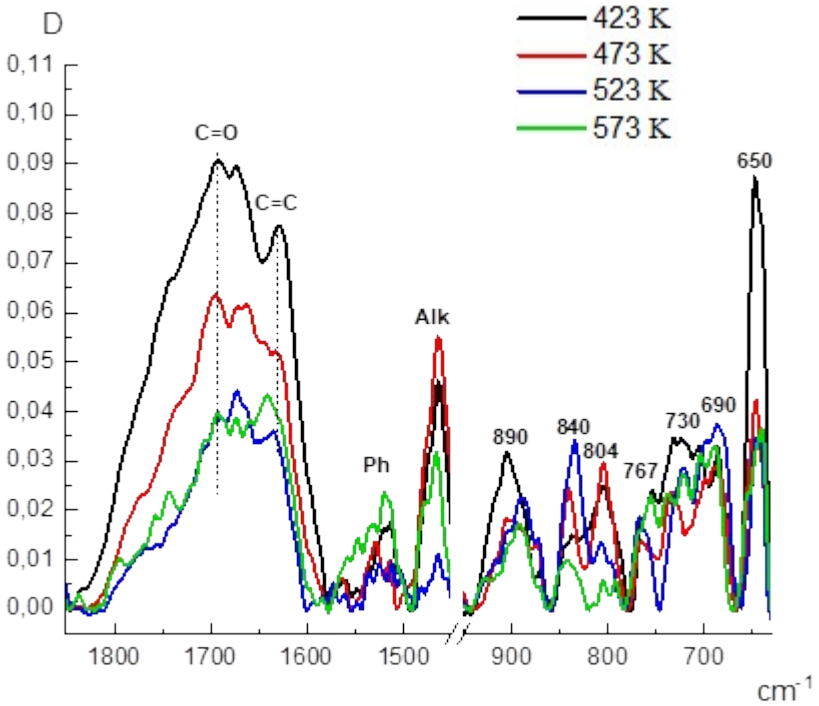

Figure S2. IR spectra of the surface of the RuO_2/ZM catalyst with DPhE +C16 in the range of 1850-600 cm^{-1}.

Since the hydrogenation of DPhE to cyclohexane proceeds faster than guaiacol, the “chair” conformation was already formed at 423 K, which was preserved over the entire temperature range.

The Ru/SBA-15 and RuO_2/SBA-15 samples were evacuated in a desiccator next to guaiacol in a watch glass. Thermogravimetric analysis (TGA) of adsorbed GUA was performed on freshly prepared samples. The integral values of desorbed organic substance were identical which meant the adsorption capacity of these samples was identical. However, the desorption peak in the case of RuO_2/SBA-15 was a little bit shifted towards higher temperature than in the case of Ru/SBA-15. That could only mean that adsorption for RuO_2/SBA-15 was advantageous.

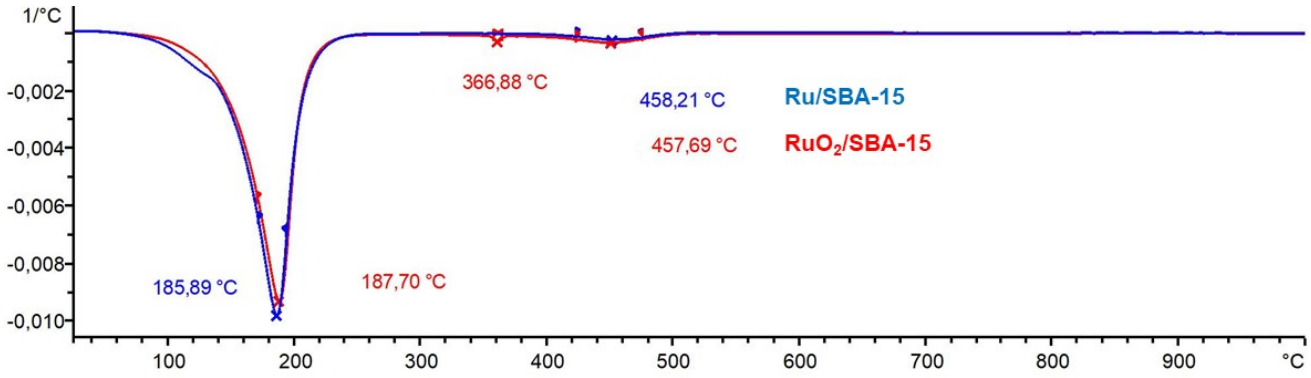

Figure S3. Differential TG curves in N_2 flow of adsorbed GUA on Ru/SBA-15 RuO_2/SBA-15

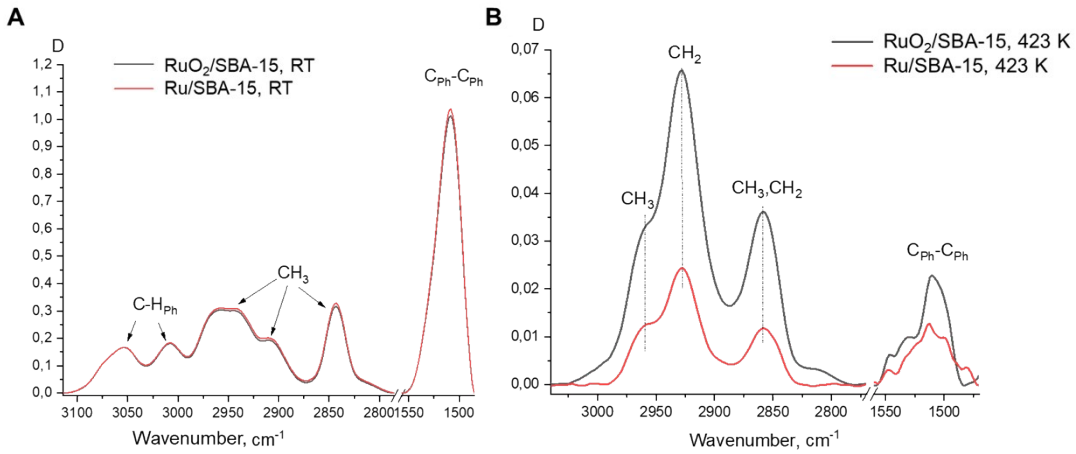

Figure S4. Differential IR spectra of adsorbed guaiacol on RuO_2/SBA-15 and Ru/SBA-15 at different temperature.

DRFIT spectra of Ru/SBA-15 RuO_2/SBA-15 with adsorbed guaiacol demonstrated that at room temperature (RT) not even a slight difference between these two samples could be seen (In Fig. S4). At 423 K, the difference in adsorption of guaiacol was significant.

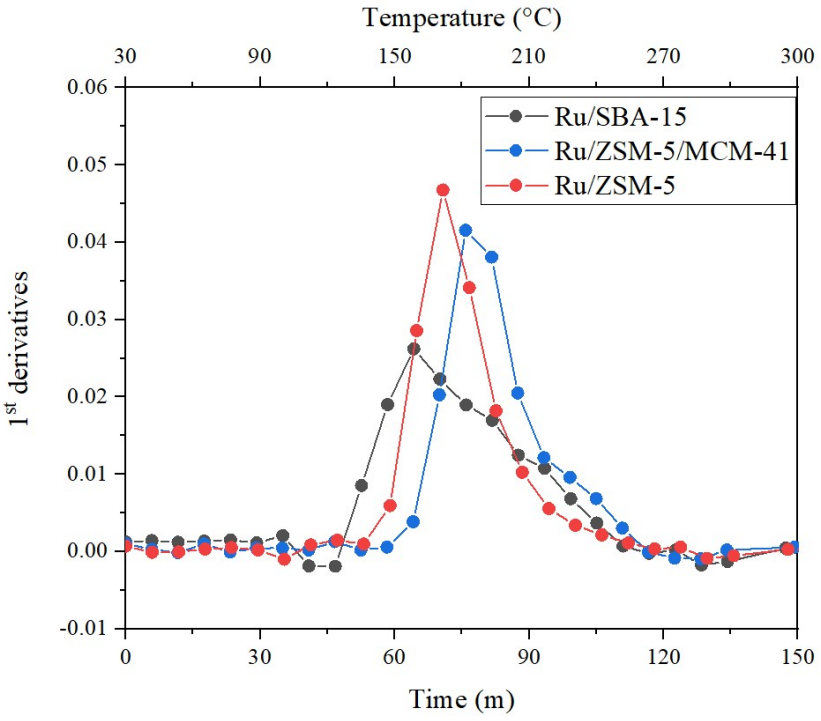

Figure S5. The 1st derivatives of evolution curve of Ru(0) and Ru(IV) phases obtained from XANES

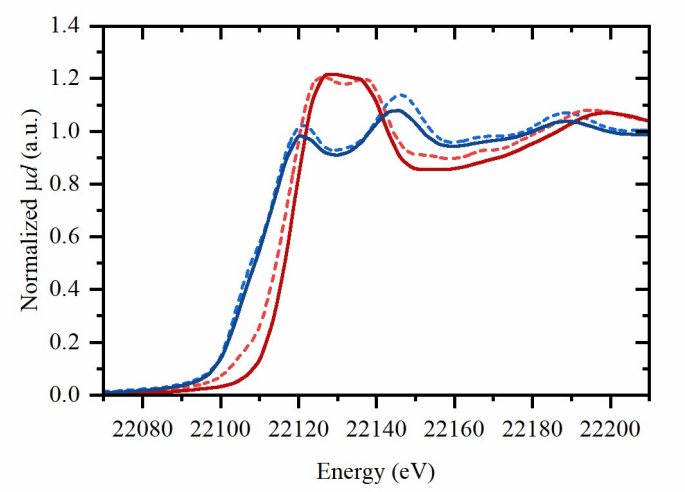

Figure S6. XANES spectra extracted by MCR analysis from the operando collected spectral data (solid lines) in comparison with the reference bulk ruthenium (IV) oxide (dashed red) and ruthenium foil (dashed blue).

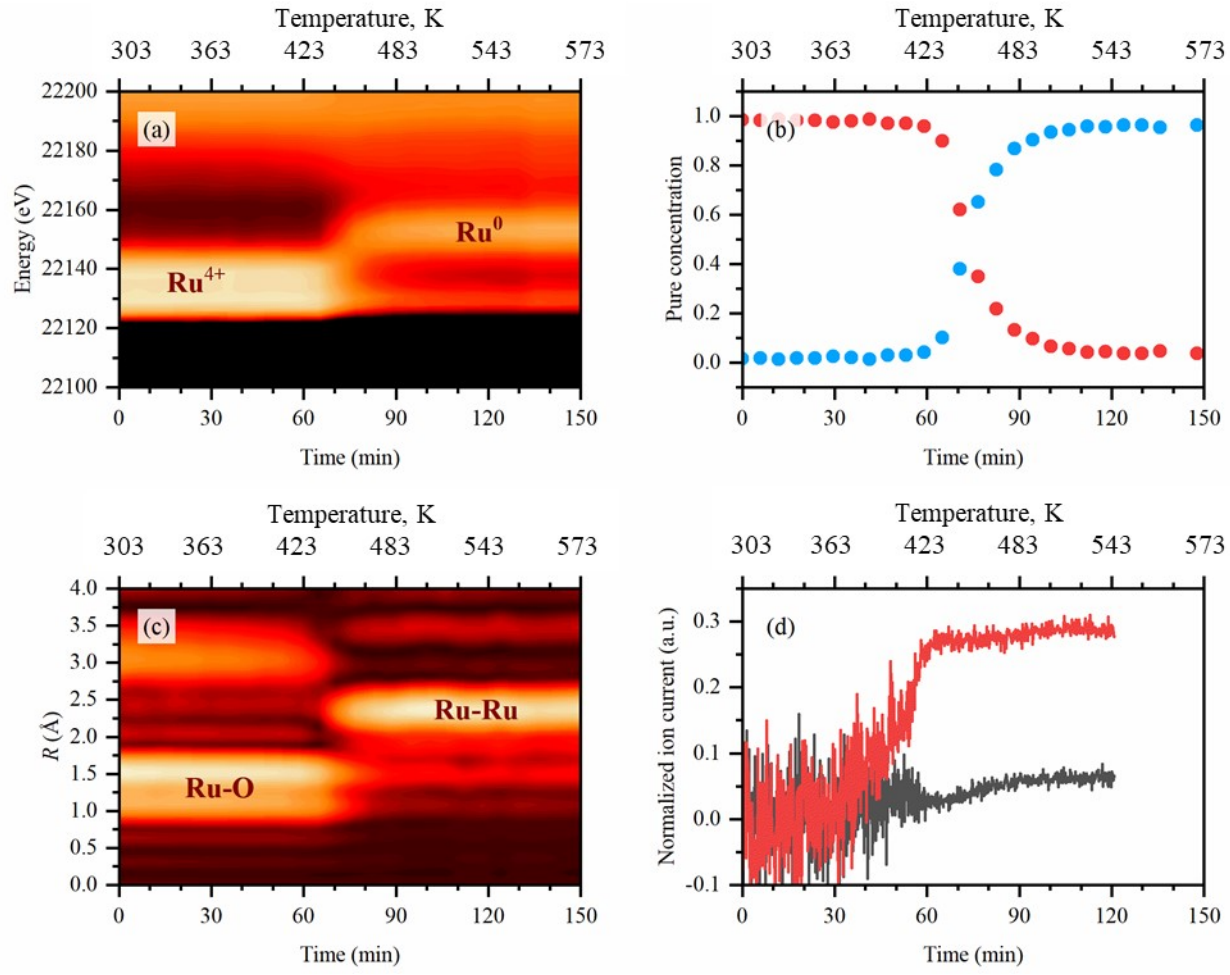

Figure S7. Summary of the *operando* XAS investigation of RuO_2/ZSM-5: (a) evolution of XANES data (color map: low intensity – black, high intensity – yellow), (b) evolution of Ru(0) (blue) and Ru(IV) (red) phases obtained from XANES, (c) evolution of phase-uncorrected FT-EXAFS data (color map: low intensity – black, high intensity – yellow), and (d) MS signals of guaiacol (black) and cyclohexane (red).

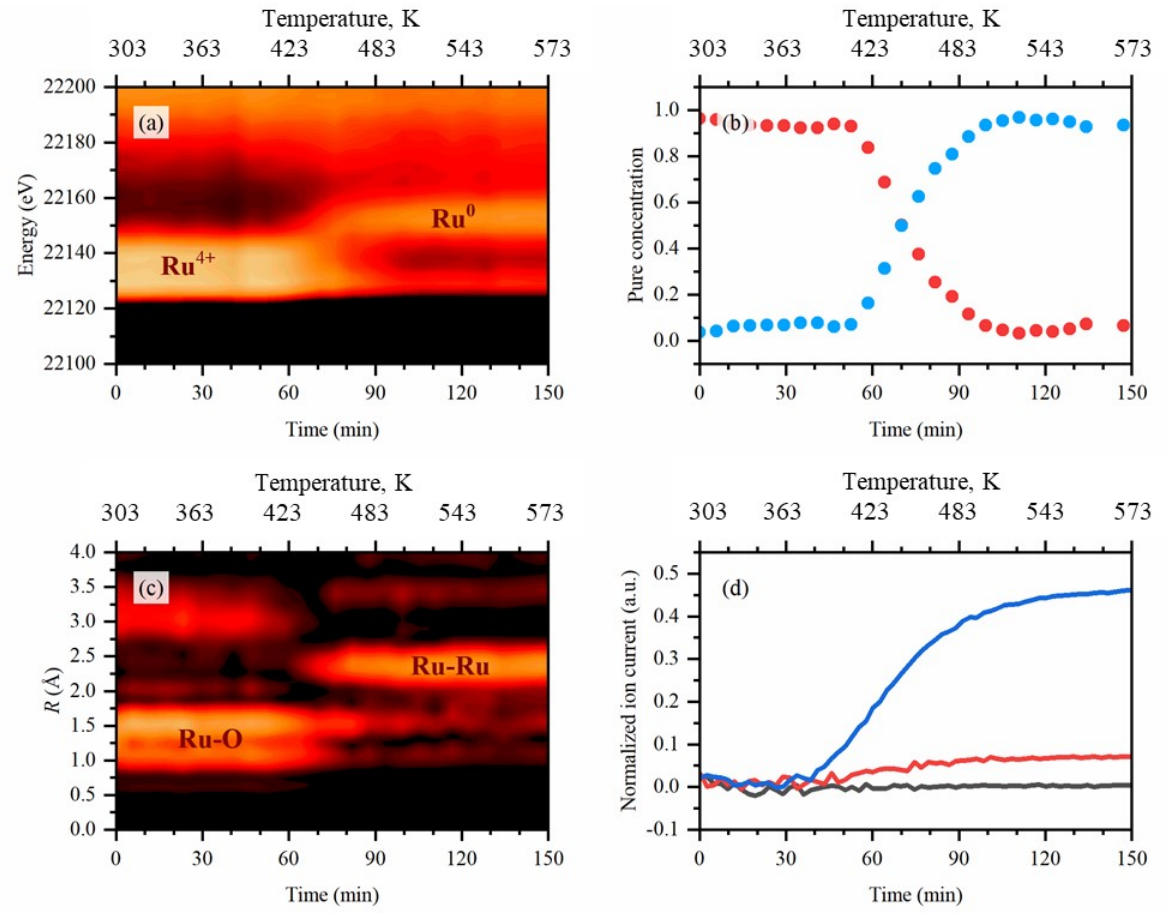

Figure S8. Summary of the *operando* XAS investigation of RuO_2/SBA-15: (a) evolution of XANES data, (b) evolution of Ru(0) and Ru(IV) phases obtained from XANES, (c) evolution of phase-uncorrected FT-EXAFS data, and (d) MS signals of guaiacol (black) and cyclohexane (red) and increase in the 1-Methoxycyclohexane (blue). The color scheme is similar as in Figure S7.

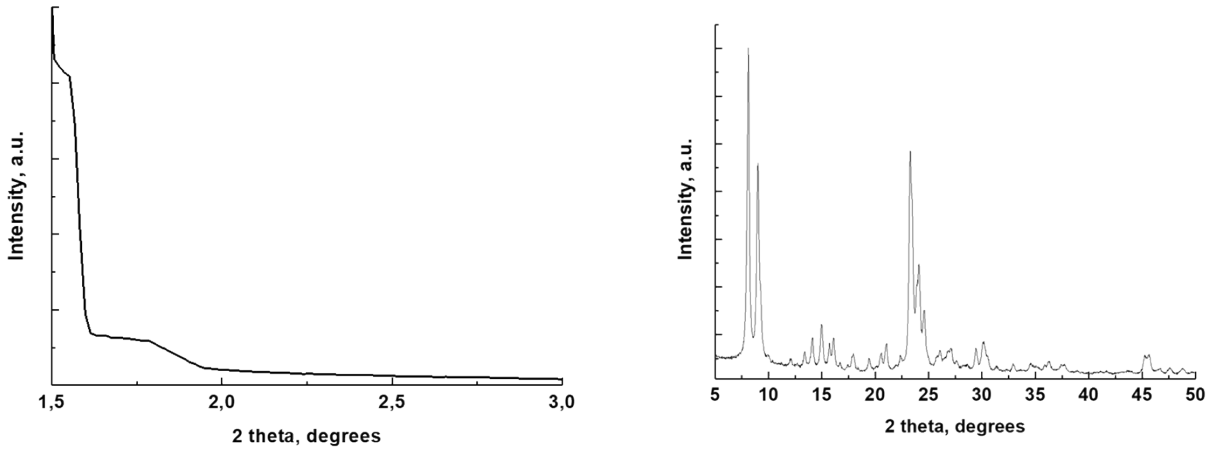

Figure S9. XRD patterns of the ZM sample

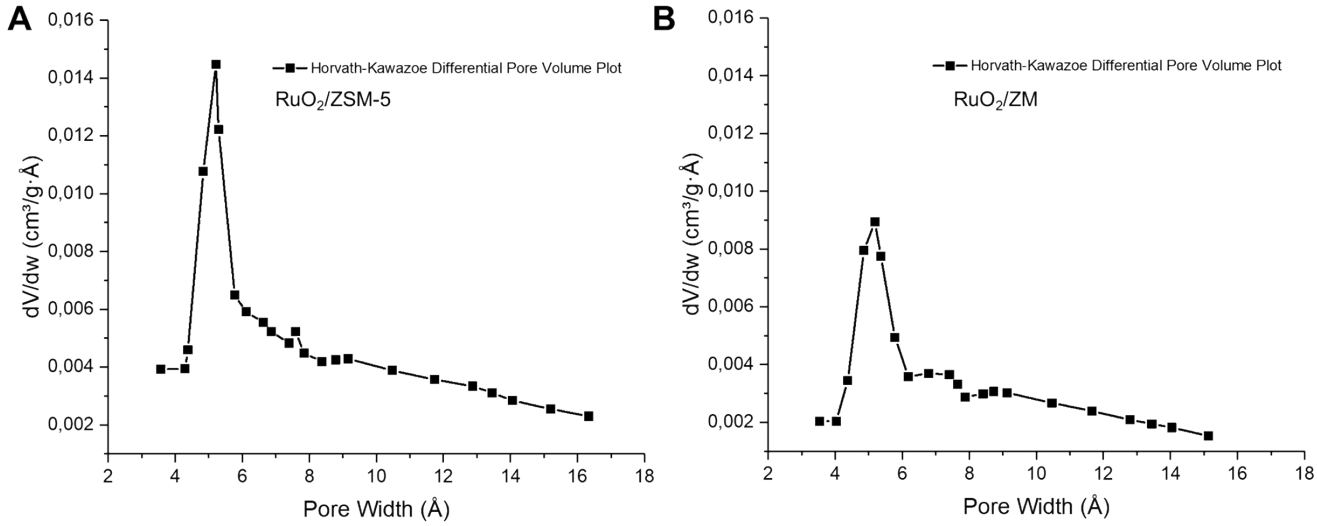

Figure S10. Pore size distribution of RuO_2/ZM and RuO_2/ZSM-5 catalysts by Horvath-Kawazoe method

References

1 M. Kruk, M. Jaroniec, Y. Sakamoto, O. Terasaki, R. Ryoo and C. H. Ko, *J. Phys. Chem. B*, 2000, **104**, 292–301.